Effect of sequential isochronal annealing on the structure and migration behaviour of selenium-ion implanted in glassy carbon

S.A. Adeojo[a,b],*, J.B. Malherbe[a], E.G.joroge[a,c], M. Mlambo[a], O.S.,Odutemowo[a], T.T. Thabethe[a], Z.A.Y. Abdalla[a], T.T. Hlatshwayo[a]

[a]Physics Department, University of Pretoria, Pretoria, South Africa
[b]Department of Physics and Engineering Physics, Obafemi Awolowo University, Ile-Ife, Nigeria
[c]ENGAGE, University of Pretoria, University of Pretoria, Pretoria, South Africa

*Corresponding author. Physics Department, University of Pretoria, Pretoria, South Africa.
u19288124@tuks.co.za

Highlights

- Selenium ions implantation at room temperature (RT) amorphized the near-surface region of the glassy carbon sample.
- Vacuum annealing of the (RT) implanted samples resulted in no diffusion at the low-temperature regime (300–700 °C).
- The diffusion of Se was observed at the high-temperature regime (1000–1200 °C).
- The Se atoms diffuse towards the surface and out of the glassy carbon substrate at 1200 °C.
- Appreciable recrystallization observed at 1200 °C indicates a partial recovery of the glassy carbon substrate.

Abstract

In a view to further study the diffusion properties of glassy carbon for its applicability as a diffusion barrier for fission products found in high-level nuclear waste, glassy carbon samples were implanted with 150 keV Se ions to a fluence of 1×10^{16} ion/cm^2 at room temperature. Some of the implanted samples were subjected to sequential isochronal annealing at two temperature regimes (300–700 °C and 1000–1200 °C) for 5 h under vacuum. Raman spectroscopy was used to investigate the structural changes while Rutherford backscattering spectrometry (RBS) was used to monitor the migration of implanted Se. Implantation of Se amorphized glassy carbon resulting in an increase in density (from 1.42 to 2.1 gcm^{-3}). No notable diffusion of Se in the glassy carbon occurred after annealing at the low-temperature regime (300–700 °C). Raman spectroscopy shows that limited recrystallization occurred after annealing at the low-temperature regime. Appreciable recrystallization coupled with some diffusion occurred at the high-temperature regime, 1000–1200 °C. The original structure of glassy carbon was not achieved after annealing at 1200 °C. Diffusion coefficients of 5.9×10^{-20} m^{2}s^{-1} and 4.79×10^{-20} m^{2}s^{-1} were obtained for Se in defective glassy carbon at 1000 and 1100 °C, respectively.

Keywords: *Implantation; Migration; Diffusion; Glassy carbon; RBS; Raman*

1. Introduction

Carbon exists in natural and synthetic forms. Glassy carbon (GC), also known as vitreous carbon is an allotrope form of synthetic carbon. It is manufactured from organic polymeric precursors through carbonization/pyrolysis processes at high-temperature (2000–3000 °C). Glassy carbon can be described as a disordered carbon material because of the absence of a long-range crystalline order within its structure. However, pockets of graphite exist within its structure [1]. Each pocket is containing an aggregate of smaller crystallites that are randomly oriented. The structure of commercially manufactured glassy carbon has been reported to contain some closed carbon nanostructure which is likened to an imperfect multilayered fullerene [2]. According to Harris, some curved graphitic layer planes were also reported within the structure of the glassy carbon [2]. A study recently carried out by Odutemowo et al. [3] agreed with Harris's study [2]. Odutemowo et al. have reported that glassy carbon contains tightly packed layered graphitic nanostructure with different orientations [3]. Also observed and reported were a few onion-like carbon microstructures (fullerenes) surrounded by mostly graphitic crystallites that are randomly oriented (the reader may refer to the HRTEM micrograph of pristine glassy carbon in [3]).

Glassy carbon has been widely explored and utilized for some industrial fabrication, some of which include electrochemistry electrodes [4,5]; crucibles [2,6], camera lenses [7], dental implant materials [8] and encapsulation materials for nuclear fuel [9,10]. The properties of glassy carbon make it suitable as a future material for the fabrication of dry casks storage systems needed for nuclear waste management. These properties include its low density (1.42–1.54 gcm^{-3}), high hardness, and strength, good electrical conductivity, extreme resistance to thermal shock, biocompatibility [11], high-temperature stability (it does not transform to graphite at temperatures of up to 3000 °C) [12], extreme resistance to chemical attack and impermeability by gases and liquids [13]. Some investigations have been done on the suitability of glassy carbon as a nuclear waste storage material. Some of these studies focused on the migration of ions implanted in glassy carbon, Be [14], Cs [15], Sr [3,16,17], In [18], Cd [19], Xe [20], Ag and Ag co-implanted Sr [21]. Only a few are on interface interaction between thin films and glassy carbon [22,23].

To the best of our knowledge, migration of selenium (Se) in glassy carbon has not been investigated so far. Selenium is a trace non-metal with atomic number 34. It has seven main natural isotopes, five (^{74}Se, ^{76}Se, ^{77}Se, ^{78}Se, and ^{80}Se) are stable and the other two (^{79}Se and ^{82}Se) are long-lived radionuclides. ^{82}Se has the longest half-life of approximately 10^{19} years. ^{79}Se can be found in minute quantities (yield of about 0.0487% [24]) in uranium ores, spent, and reprocessed nuclear fuel. The neutron activation of ^{78}Se can also lead to the production of ^{79}Se [25]. The decay of ^{79}Se gives rise to the release of beta particles with an average energy per decay of about 0.0053 MeV [26]. Its long half-life of 327,000 years makes it a potential index to determine the long-term radiological assessments of a geological repository on the environment [27]. The migration of ^{79}Se in the biosphere is expected to be identical to other nonradioactive selenium [25]. Any quantity of ^{79}Se can be leaked from geological repositories, then accumulated and transported through different environmental media (soil, sediments and water) to man and animals. Food crops tend to have a low tolerance of selenium [28] but can accumulate a level of selenium that would be toxic to man and animals [29]. Cancer can be induced consequent to selenium toxicity, especially when ingested into the body at a dose >400 μg per day [30].

Our group at the University of Pretoria, South Africa has been studying the diffusion of fission products in glassy carbon in the last decade [3,[15], [16], [17], [18], [19], [20], [21], [22], [23]]. To add to the existing studies, we have investigated the migration of non-metallic fission product, Se in glassy carbon. To this end, Se ions was implanted in glassy carbon substrates to a fluence of 1×10^{16} ion/cm^2 at room temperature (RT) to investigate the effects of radiation damage on the glassy carbon structure. The implanted samples were subjected to heat treatment in vacuum to study the migration behaviour of Se^+ implanted in glassy carbon. The structural changes of glassy carbon was also investigated in the implanted and then heat-treated samples.

2. Experiment and analysis

The starting material was commercial SIGRADUR® G glassy carbon strips purchased from Hochtemperatur-Werkstoffe GmbH, Germany. Each strip of dimension 50 mm × 10 mm × 2 mm was mechanically polished to a mirror finish with a 1 μm diamond solution. The unpolished surface of the glassy carbon strip was marked into 10 rectangular wafers. Each wafer had a dimension of 5 mm × 10 mm × 2 mm. A cut (of few microns) was made at the mark separating each cell. This cut was to ensure the easy separation of the glassy carbon into wafers after ion implantation. The glassy carbon samples were sequentially cleaned in a soap solution, de-ionized water, and methanol, in an ultrasonic bath and later dried using nitrogen gas. Three cleaned glassy carbon strips were implanted simultaneously with 150 keV Se ions to a fluence of 1×10^{16} ion/cm^2 at room temperature. Uniform implantation was ensured by scanning the Se beam across each glassy carbon strip. During implantation, the flux was maintained at about 10^{13} cm^{-2}s^{-1} to minimize beam induced substrate heating. After implantation, the glassy carbon strips were easily separated into 30 wafers (10 per strip).

To investigate the migration behaviour of Se and annealing of radiation damage, some of the implanted glassy carbon wafers were heat-treated under vacuum conditions using two different vacuum annealing systems: a quartz tube furnace (for the low-temperature regime) and a computer-controlled Webb 77 graphite furnace (for the high-temperature regime), respectively. A sample was first subjected to sequential isochronal annealing between 300 and 700 °C in steps of 100 °C in the quartz tube furnace. The Webb 77 graphite furnace was used for the sequential isochronal annealing of another implanted sample at 1000–1200 °C in steps of 100 °C. The annealing duration at each temperature (i.e. at each annealing step) was 5 h. In both annealing systems, precautions were taken to maximally reduce sample contamination by residual gas and/or particles. Before and after each annealing cycle in the quartz tube furnace, the tube and other components were thoroughly cleaned with acetone and blown with nitrogen gas. Also, once the sample was placed inside the quartz tube, a fore pump was operated to evacuate the tube up to 10^{-3} mbar range and then the turbo pump was started to provide a high vacuum to about 10^{-7} mbar range. Before using the Webb 77 graphite furnace, the furnace was evacuated to about 10^{-7} mbar using a mechanical pump coupled with a turbo pump. The pumping was followed by an outgassing phase where the furnace is heated to 100 °C for like 3 h. The outgassing process was expected to reduce the gas contaminants and desorbed water vapour that may have been adsorbed onto the furnace's internal insulation material. The implanted sample was then placed inside a graphite crucible before annealing in the Webb furnace. The details of annealing set-ups and procedures can be found in [31].

The depth profiles of Se implanted in glassy carbon before and after annealing were measured by Rutherford backscattering spectrometry (RBS). The RBS measurements were performed using helium ($^4He^+$) particles of 1.3–1.6 MeV energy with a beam current of 15 nA. The backscattered particles were detected by a silicon surface barrier detector at a backscattering angle of 165°. The ion beam current was measured on the sample and a ring-shaped electrode in front of the sample was kept at −200 V to suppress ejected secondary electrons and an 8 μC charge was collected per measurement. Simulation of the implanted ions was performed using SRIM-2010 [32]. Since previous studies have shown that ion implantation at room temperature to a fluence in the same order as used in this study, amorphized glassy carbon leading to a change in the density of the substrate [3,33], it is important to estimate the new density of the implanted glassy carbon material using the method described in reference [3]. The new density of Se implanted glassy carbon was then calculated to be 2.1 g/cm^3 (10.5×10^{22} atoms/cm^3), which was used in the SRIM simulation. The RBS Se profiles in energy/channel were converted into depth profiles using the energy loss data and density of the amorphized glassy carbon, 10.5×10^{22} atoms/cm^3.

The structure of the glassy carbon before implantation, the radiation damage retained after implantation, and the effect of annealing were investigated using Raman spectroscopy. The Raman instrument consisted of a T64000 series II triple spectrometer system from HORIBA scientific, Jobin Yvon Technology; a coherent Innova 70C® series Ar^+ laser (using the 514.5 nm laser line) and an Olympus microscope (the 50

objective lens was used). The integrated triple spectrometer was used in the double subtractive mode to reject the Rayleigh scattering and disperse the light onto liquid nitrogen cooled Symphony CCD detector. During the Raman measurement, it was important to keep the laser power below 1 mW to minimize sample heating.

3. Results and discussion

Fig. 1 shows the RBS experimental spectrum of room temperature as-implanted glassy carbon. The respective surface channel position of C and Se are indicated by the arrows and the Se profile has a Gaussian distribution. Fig. 2 shows the experimental depth profile of 150 keV Se ion-implanted in glassy carbon, simulated distribution, and the simulated damage in displacement per atom (dpa). The simulation was carried out using SRIM and taking the threshold displacement energy of C as 20 eV [34]. The experimental depth profile of Se was fitted to a Gaussian equation and an average projected range (R_p) and straggling (ΔR_p) was estimated as 84 and 29 nm. The experimental R_p is comparable with the SRIM prediction of 89 nm. The difference between the two R_p values is within 5–10% uncertainties of SRIM simulations. The experimental projected range straggling overestimates the SRIM calculation of 20 nm by 31%. Previous studies on ion implantation in glassy carbon have shown that experimental projected range straggling usually overestimates the SRIM prediction, by factors such as 43% for Sr [17], 23% for In [18] and 38% for Xe [20]. The underestimation in the theoretical straggling is not strange owing to several approximations used in the SRIM program.

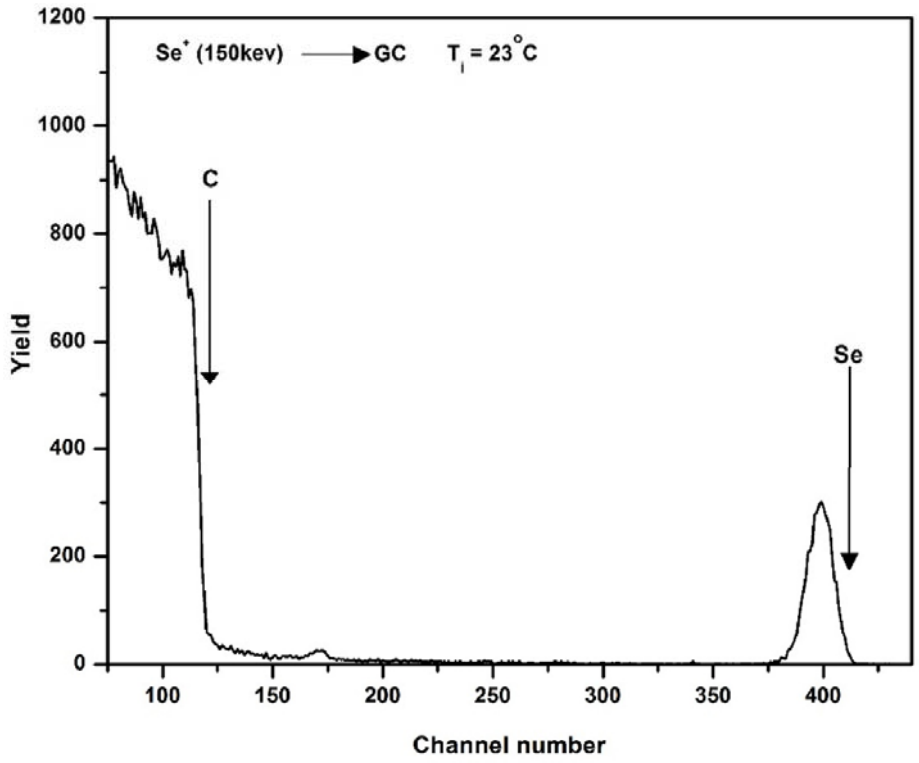

Fig. 1. Rutherford backscattering spectrometry (RBS) spectrum of room temperature as-implanted glassy carbon.

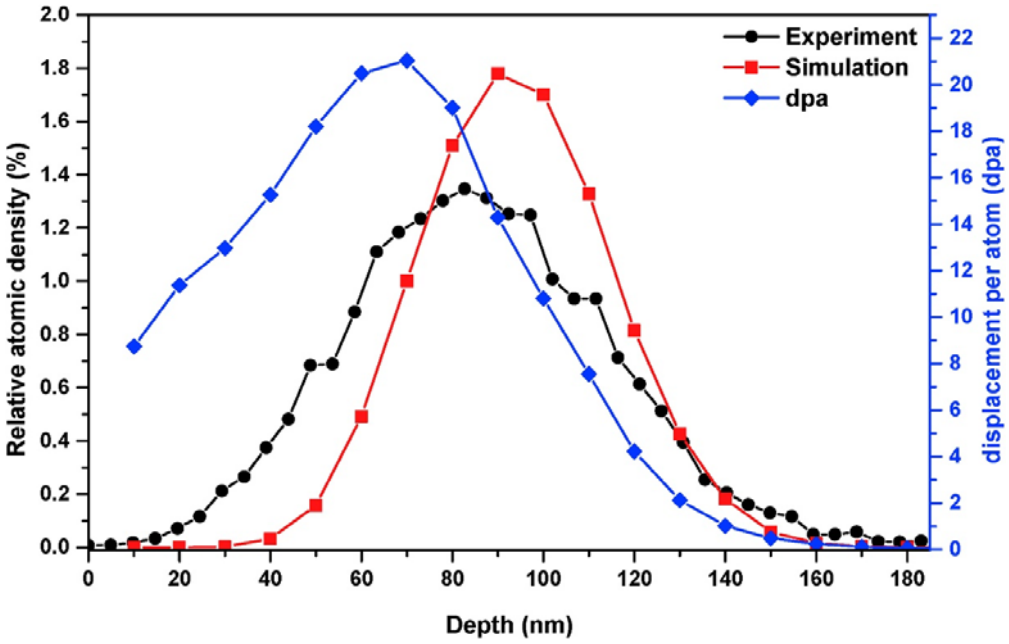

Fig. 2. RBS depth profile of Se implanted at room temperature (circles) compared with SRIM simulated Se depth profile (squares) and the damage in displacement per atom (dpa) (diamonds).

The fluence of implanted Se ions was converted into displacements per atom (dpa) using equation (1) [19].

$$dpa = \frac{\text{Vac/(ion Å)} \times 10^8}{\rho_{GC}(atoms\ cm^{-3})} \times \varphi\,(ions\ cm^{-2}) \quad (1)$$

Åwhere V_{ac}/(ion Å) represents the number of vacancies per ion per Angstrom, 10^8 is the conversion factor from Angstrom to a centimeter, φ is the ion fluence – (1.0×10^{16} ions cm^{-2}) and ρ_{GC} is the density of Se implanted glassy carbon – (10.5×10^{22} atoms/cm^3).

The maximum damage level of 21 dpa obtained in this study is higher than the critical value of about 0.2 dpa required for the amorphization of typical glassy carbon [35]. The radiation damage created in the glassy carbon is maximum at a depth of 70 nm below the surface. This means that the majority of the radiation damage is towards the surface rather than deeper to the bulk of the glassy carbon. Assuming a critical dpa of 0.2, the thickness of the amorphous layer was estimated to be 160 nm from Fig. 2. Hence the implanted Se is embedded in the amorphous region.

Fig. 3(a) shows the Raman spectrum of a pristine glassy carbon. The spectrum has two pronounced asymmetric peaks at about 1352 cm^{-1} (D peak) and 1588 cm^{-1} (G peak) wavenumbers, respectively. The D peak was attributed to the Raman breathing mode of A_{1g} symmetry (six-fold aromatic ring) involving phonons at the K zone boundary [36]. The D peak is forbidden in perfect graphite and only found in disordered carbon [36]. The G peak is due to Raman optical phonon mode combined with E_{2g} symmetry [37,38]. One other peak identified as D' at 1620 cm^{-1} is usually found in pristine glassy carbon. The peak is a defect induced Raman feature which is evidence of very small-sized graphitic grains found in glassy carbon [36,38]. It must be stressed that the D' peak is absent in highly crystalline graphite [39].

The Raman spectra of the pristine glassy carbon, as-implanted and annealed samples were fitted using the Breit-Wigner-Fano function (for the G peak) and a Lorentzian function (for the D peak). The fitting enabled us to obtain information such as the peak position and intensities, area, and the full width at half maximum (FWHM) of the D and G band. The crystallite size of the SIGRADUR ® G pristine glassy carbon was calculated using equation (2) [40]. The Tuinstra–Koenig relation is valid in estimating the average crystallite size (L_a) of any form of graphitic carbon over the range of 2 nm < L_a < 30 nm [36].

$$\frac{I_D}{I_G} = \frac{C_\lambda}{L_a} \quad (2)$$

I_D/I_G is the D to G peak intensity ratio, determined to be 1.43 for the pristine glassy carbon, C_λ is the laser excitation wavelength-dependent constant taken as 44 Å for 514.5 nm excitation laser line [40], L_a is the average crystal size of the pristine glassy carbon and it was calculated to be 3.1 nm. With this value of crystallite size, 3.1 nm, glassy carbon can be classified as nano-crystalline graphite [39].

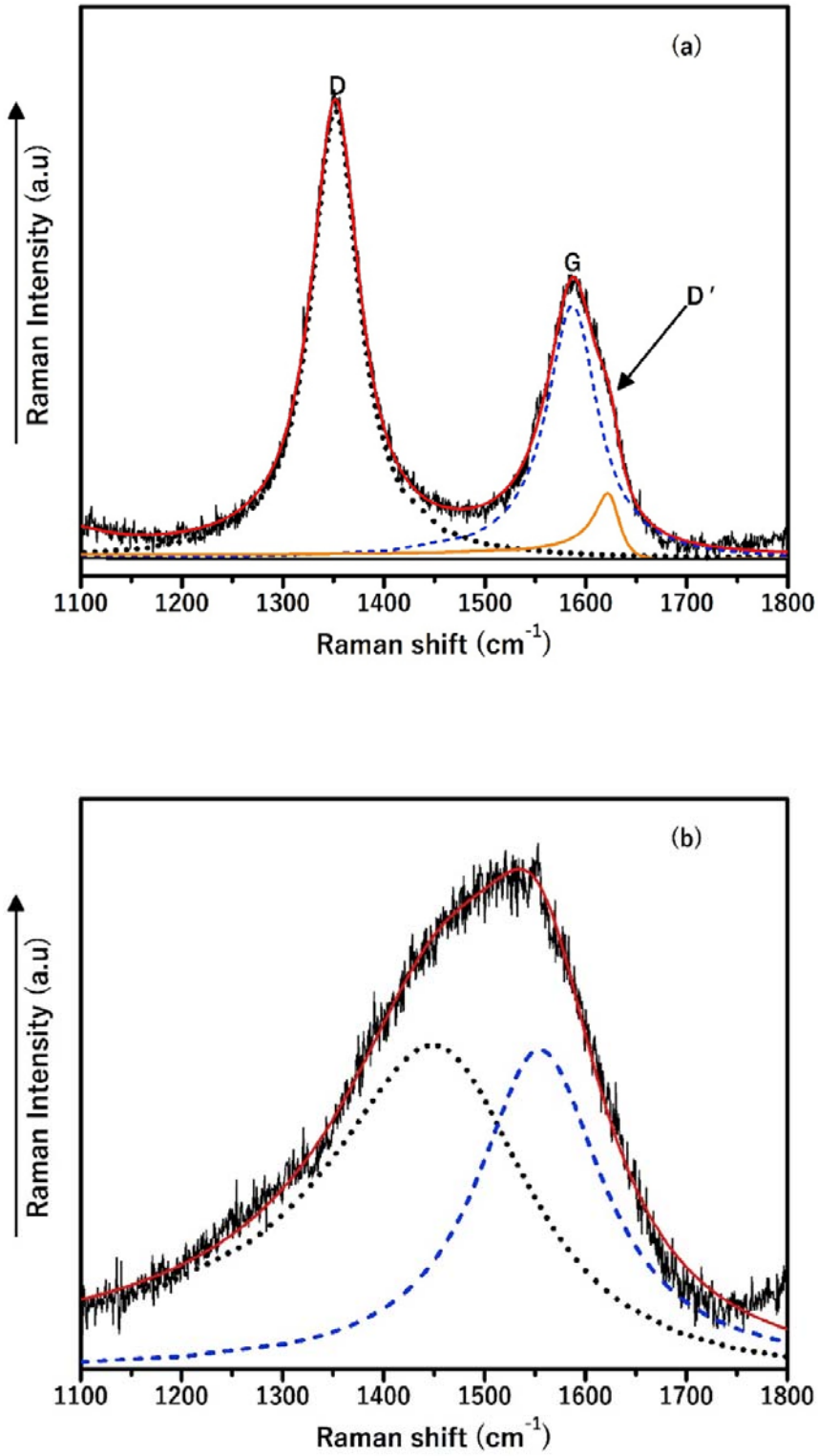

Fig. 3. Raman spectra of (a) pristine glassy carbon and (b) Se implanted in glassy carbon at room temperature. The cumulative fit peak (solid red line), G peak fit (black dotted line), D peak fit (blue dashed line) and D' peak fit (orange solid line).

Implantation of Se ions into glassy carbon resulted in the merging of D and G peaks displayed as a broad peak around 1449–1555 cm^{-1} in Fig. 3(b). After the deconvolution of the broad spectrum in Fig. 3(b), two individual peaks (i.e. the D and G peaks) were identified. The G peak has shifted to lower wavenumber (from 1588 to 1554 cm^{-1}) accompanied by the G peak broadening and a decrease in D peak and G peak intensity ratio (I_D/I_G), from 1.43 to 1.01. These changes observed in the Raman features in Fig. 3(b) reflect the transformation of glassy carbon into an amorphous form. Using the amorphization trajectory proposed by Ferrari and Robertson [36], the I_D/I_G ratio can be related to sp^2 and sp^3 bonds in carbon materials and the drop of I_D/I_G from 1.43 to 1.01 suggests that 15% of sp^2 bonds were converted to sp^3 bonds. The Tuinstra–Koening relation, equation (2), breaks down after ion implantation into the glassy carbon [36]. The Tuinstra–Koening equation presumes that the I_D/I_G is proportional to the number of rings at the edge of the grains [36]. With the loss of some sp^2 rings in the amorphized glassy carbon, the D peak intensity will decrease with respect to the G peak intensity as a function of disorder and the Tuinstra–Koening relation no longer holds. Another relation, equation (3) was proposed by Ferrari and Robertson to estimate the average crystallite size of amorphized carbon [36].

$$\frac{I_D}{I_G} = C'_\lambda \, L_a^2 \tag{3}$$

where C'_λ is a constant taken as 0.0055 $Å^{-2}$ [36], L_a is the average crystallite size and I_D/I_G carries the usual meaning already stated above. The calculated average crystallite size for the pristine glassy carbon, 3.1 nm reduces to 1.36 nm after Se ion implantation at room temperature. The high fluence (1×10^{16} ions/cm^2) of Se ion implantation partially destroyed the graphite crystallites in the implanted region of the glassy carbon thereby leading to reduced crystallite sizes. This implies that aside from the G peak downward shift, the G peak broadening and the decrease in I_D/I_G ratio, the reduced average crystallite size is another evidence that Se ion implantation damaged the glassy carbon structure. This leads to having a highly disordered region (with bond angle disorder) within the glassy carbon substrate. It is interesting to note that the Co and In ions implantation into glassy carbon at a fluence in the same order of magnitude (i.e. 10^{16} ions/cm^2) used in this study has been characterized with different average crystallite sizes, 1.1 nm for 150 keV Co^+ [41] and 1.3 nm for 360 keV In^+ [18] as compared to the crystallite size of Se in this study. The variation in the crystallite sizes might be due to the different atomic masses of these elements.

Fig. 4, Fig. 5 show the Raman spectra of Se implanted glassy carbon after annealing at low (300–700 °C) and high (1000–1200 °C) temperature regimes, respectively. The Raman spectra of the samples annealed at 300 to 400 °C are not different from the as-implanted Raman spectrum indicating insignificant recrystallization after annealing at these temperatures. The Raman spectrum obtained after annealing at 500 °C is different from the as-implanted Raman spectrum, as the D and G peaks are slightly distinguishable. Hence, the 500 °C annealing temperature can be considered as a critical temperature where the defects within the implanted region became thermally activated and began to anneal out. As the annealing temperature was increased from 500 °C, the peaks grow in intensities and at the highest annealing temperature, 1200 °C, the D and G peaks are well distinguished. The gradual increase in the D and G peak intensities is an indication of progressive annealing of defects which could depict an increase in graphitic order within the implanted region of the glassy carbon.

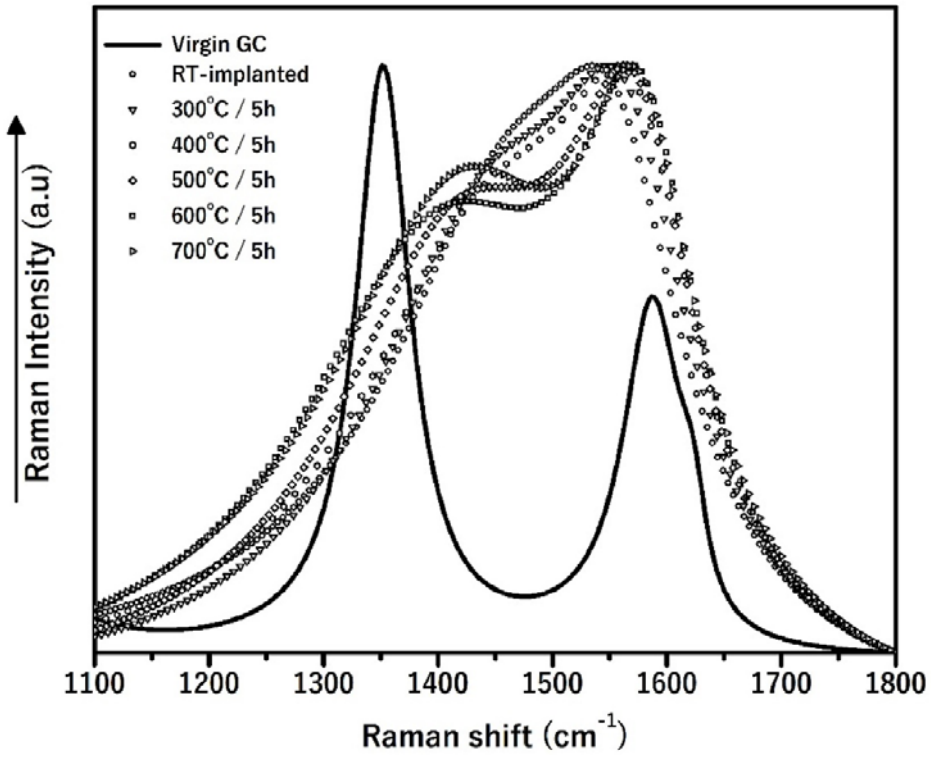

Fig. 4. Raman spectra of pristine glassy carbon after Se implantation and sequential isochronal annealing at the low-temperature regime (300–700 °C) for 5 h.

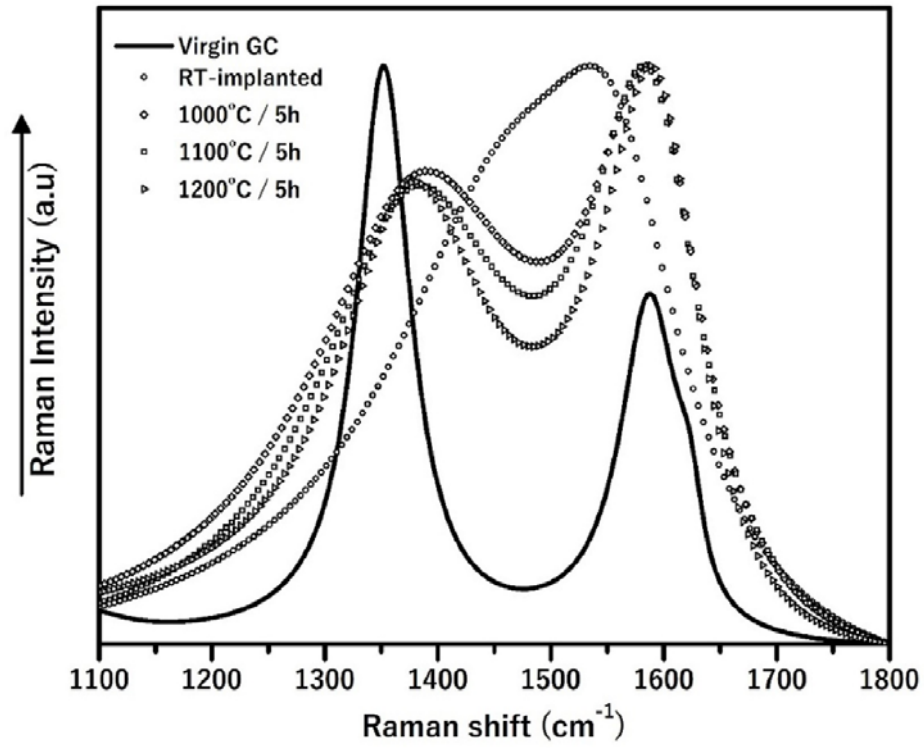

Fig. 5. Raman spectra of pristine glassy carbon after Se implantation and sequential isochronal annealing at the high-temperature regime (1000–1200 °C) for 5 h.

Parameters such as the D and G peak heights, G peak position, and FWHM were extracted from the deconvoluted Raman spectra. The G peak position, G peak FWHM, I_D/I_G ratio, and L_a variation with annealing temperature are plotted in Fig. 6, Fig. 7. These parameters were used to obtain structural information about the effect of annealing on the as-implanted samples. The G peak position shifts upward progressively from about 1440 cm^{-1} at 300 °C to a maximum of 1588 cm^{-1} at 1200 °C. This continuous upward shift in the G peak position was accompanied by a progressive decrease in the G peak FWHM in respect of increase in the annealing temperature (i.e. from 151.0 to 123.9 cm^{-1} and 118–112.1 cm^{-1} for the samples annealed at 300–700 °C and 1000–1200 °C, respectively). The D to G peak intensity ratio (I_D/I_G) decreased from the as-implanted value, 1.01 to 0.84 after annealing the as-implanted sample from 300 to 700 °C, and progressively decreased from 0.79 to 0.72 after annealing the as-implanted sample from 1000 to 1200 °C (see Fig. 7). One would expect that annealing will lead to recrystallization within the implanted region of the glassy carbon. To check for recrystallization, the average crystallite size, L_a (as a function of annealing temperature) was estimated using the Tuinstra-Koenig relation, equation (2). The choice of Tuinstra-Koenig equation was based on an assumption that as the I_D/I_G ratio decreases, the crystallite size will increase with respect to annealing. The graphite crystallite sizes obtained ranged from 4.75 to 5.21 nm and 5.57–6.07 nm for the samples annealed at 300–700 °C and 1000–1200 °C, respectively (see Fig. 7). The L_a values are within the range of 2 nm < L_a < 30 nm where the Tuinstra–Koenig relation applies for carbon materials (GC in this case). The average crystallite sizes have grown larger compared to those found in pristine glassy carbon (L_a = 3.1 nm) and the as-implanted sample (L_a = 1.36 nm). The increase in the average crystallite size with increasing temperature (for the two annealing regimes) is in line with the crystal growth theory [42].

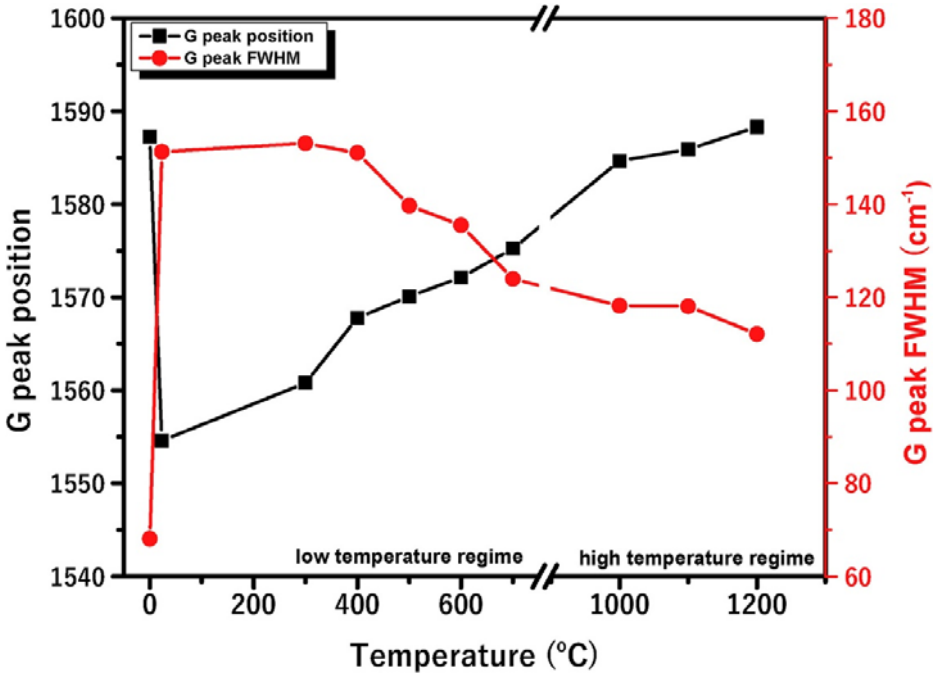

Fig. 6. G peak position (black squares) and G peak bandwidth (FWHM) (red circles) of Raman spectra of pristine glassy carbon (first point), after implantation and after sequential isochronal annealing at the low and high-temperature regimes.

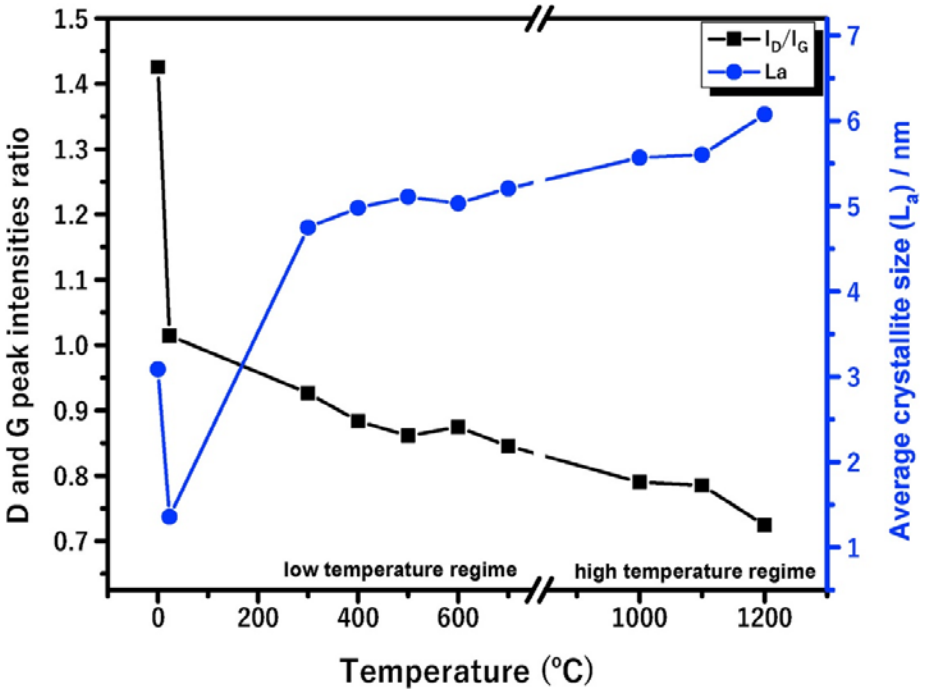

Fig. 7. I_D/I_G ratio (black squares) and crystallite size (L_a) (blue circles) of Raman spectra of pristine glassy carbon (first point), after implantation and after sequential isochronal annealing at the low and high-temperature regimes.

The gradual upward shift in the G peak position with increasing annealing temperature indicated a regrowth of the crystallites into larger sizes in line with the above calculations. The narrowing of the G peak FWHM can also be attributed to the decrease in bond angle disorder [43]. It is important to note that the G peak FWHM did not return to its original value (68.1 cm^{-1} for the pristine glassy carbon) at the highest annealing temperature of 1200 °C. This is an indication that annealing only resulted in partial recovery of the glassy carbon substrate and some radiation damage was retained in the glassy carbon structure at 1200 °C. It has been pointed out that the heat treatment of amorphized carbon materials does not usually remove all radiation damage [[18], [19], [20],43]. All the changes recorded in the G peak position, FWHM, I_D/I_G and L_a (after annealing) is evidence that annealing decreased the disorder in the implanted damaged region which resulted in recrystallization within the glassy carbon substrate. It must be stated only that limited recrystallization occurred at the low-temperature regime (300–700 °C) and appreciable recrystallization was observed at the high-temperature regime (1000–1200 °C). Recrystallization of amorphized glassy carbon due to annealing has been reported in other studies [[17], [18], [19],43].

The diffusion of implanted Se was investigated by comparing the square of the full width at half maximum ($FWHM^2$) of the depth profiles of Se from the as-implanted and annealed samples. This is because the broadening of a profile indicates the diffusion of implanted ions [44]. The FWHM was obtained by fitting the depth profiles in Fig. 8, Fig. 9 to a Gaussian function. Peak positions and $FWHM^2$ as a function annealing temperature are shown in Fig. 10. The amount of retained Se was calculated by taking the ratio of the areas under each Se profile (after each annealing step) to that of the as-implanted profile. The retained ratio as a function of annealing temperature is shown in Fig. 11.

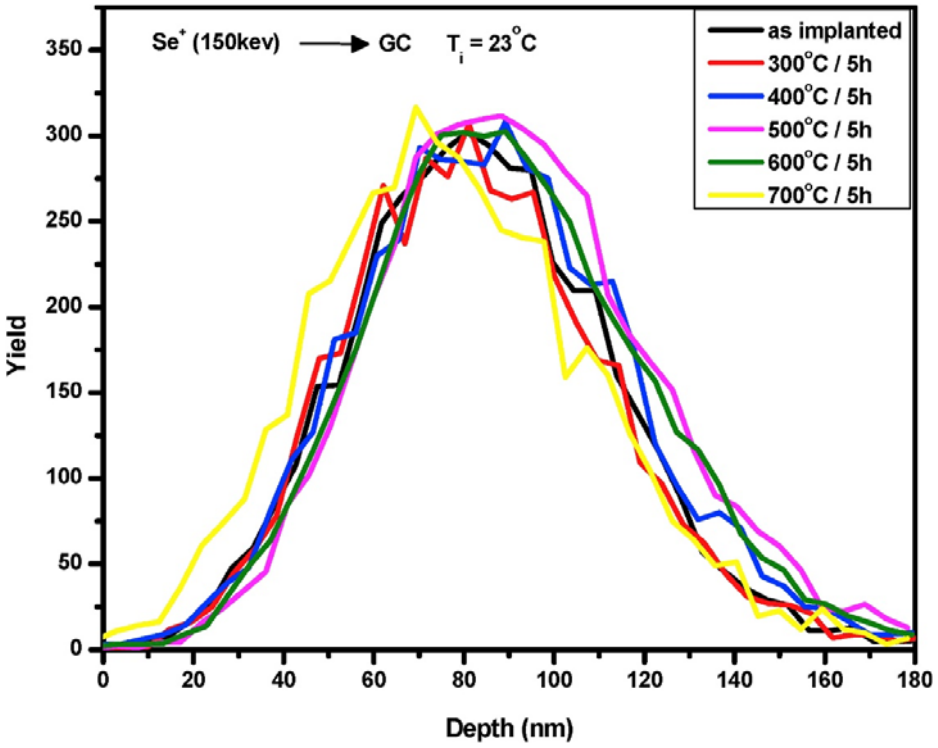

Fig. 8. Depth profiles of 150 keV Se ion-implanted in glassy carbon and after sequential isochronal annealing at the low-temperature regime (300–700 °C) for 5 h.

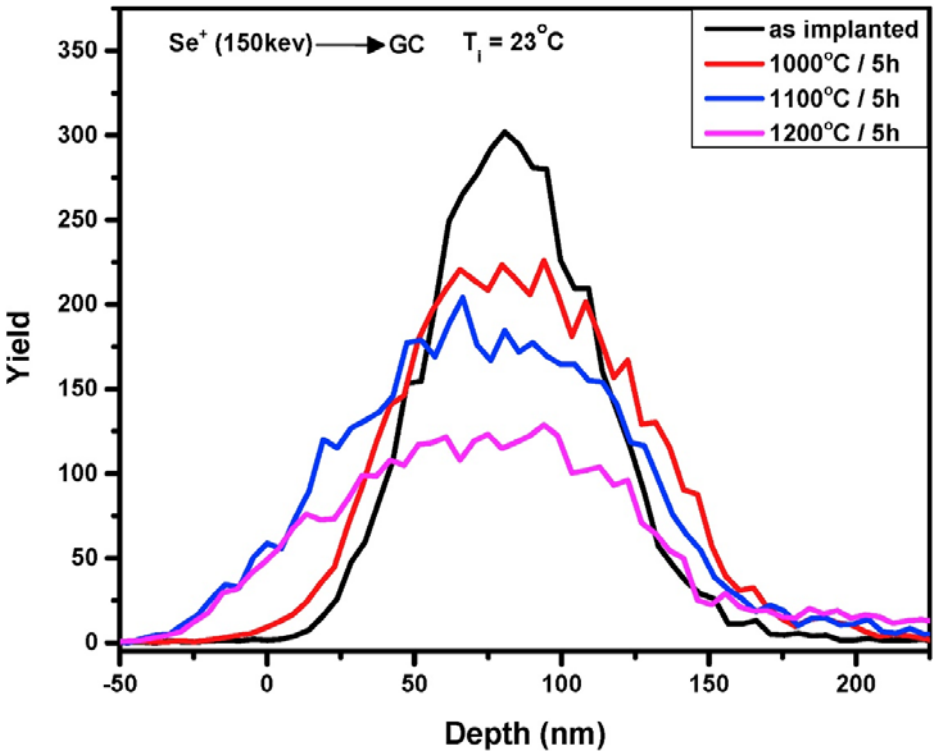

Fig. 9. Depth profiles of 150 keV Se ion-implanted in glassy carbon and after sequential isochronal annealing at the high-temperature regime (1000–1200 °C) for 5 h.

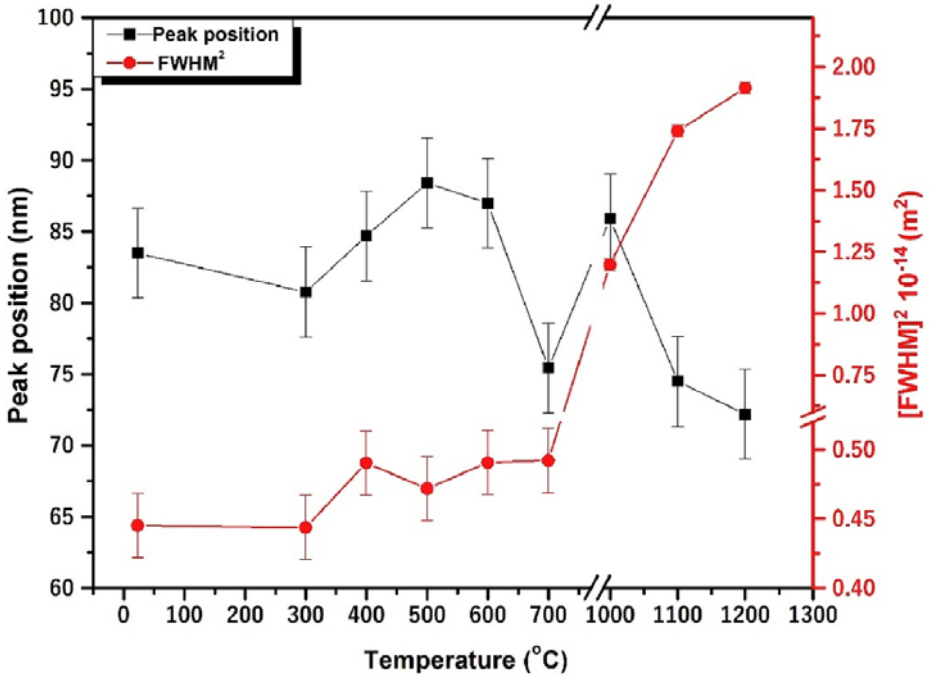

Fig. 10. Peak position (squares) and full width at half maximum (circles) of 150 keV Se ion-implanted in glassy carbon and after sequential isochronal annealing at the low (300–700 °C) and high (1000–1200 °C) temperature regimes for 5 h.

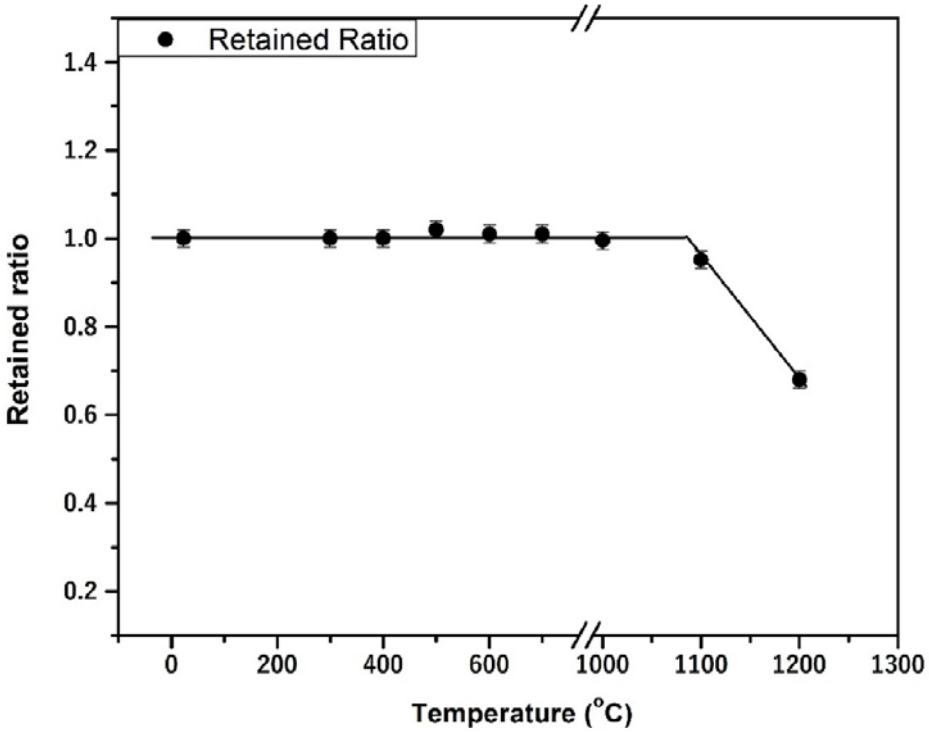

Fig. 11. The retained ratio of Se (calculated as the ratio of the total areas under each Se profile (after each annealing step) to that of the as-implanted profile) as a function of low (300–700 °C) and high-temperature annealing regimes (1000–1200 °C).

To investigate the diffusion behaviour of Se implantation in glassy carbon at the low-temperature regime, a room temperature implanted sample was subjected to sequential isochronal annealing from 300 to 700 °C in steps of 100 °C for 5 h. The RBS depth profiles were measured after each annealing step of 100 °C. Fig. 8 shows the RBS Se depth profiles. The Se profiles at 300–700 °C were essentially the same as the as-implanted profile. The variation in the $FWHM^2$ and the peak positions of the sample annealed at 300–700 °C are within the experimental uncertainty of the depth scale of the RBS measurements (see Fig. 10). The measurement error in the $FWHM^2$ was estimated from the standard deviation in the $FWHM^2$ using the data up to 600 °C. The measurement error in the peak positions was obtained from the standard deviations of the peak position of the implanted Se peaks and the surface positions of the carbon RBS peak. These two standard deviations were added in the normal way. There is no physical reason why the implanted Se peak position would change due to annealing. However, changes can occur when Se is lost due to out-diffusion. Due to the fitting of a Gauss function to the limited data, there is also a possibility the fitting might not give an exact position. For the standard deviation calculations of the peak positions, only the data up to 600 °C were used.

As was mentioned above, there was no notable diffusion for the sample annealed at the low-temperature regime (300–700 °C). There was also no loss of Se atoms from the glassy carbon substrate during annealing in the low-temperature regime (see Fig. 11). Following the non-diffusion of the Se atoms in glassy carbon at the low-temperature regime, another RT implanted sample was sequentially annealed at the high-temperature regime from 1000 to 1200 °C in steps of 100 °C for 5 h (see Fig. 10 for the depth profile). Annealing at 1000 °C led to the broadening of the Se depth profile with tailing on both sides. This broadening means that there was some diffusion of Se in the glassy carbon at this temperature, 1000 °C. The Se profile broadening became pronounced after annealing at 1100 °C. This broadening was accompanied by a peak shift from 84 to about 75 nm at 1100 °C. This implies that the implanted Se has diffused towards the surface of the glassy carbon resulting in a loss of about 5% Se atoms that reached the surface (i.e. at $x = 0$) after annealing at 1100 °C (see Fig. 11). Annealing at 1200 °C showed further broadening of Se profile accompanied by a loss of about 32% Se atoms (Fig. 11) and further peak shift (from 75 to 72 nm) towards the surface. Evaporation of the Se into the vacuum is possible when the atoms reach the surface because the low melting point of Se, of 220 °C, is significantly less than the sample annealing temperature of 1000–1200 °C.

The diffusion coefficients of Se within the defective glassy carbon were estimated by fitting the RBS depth profiles data (Se implanted at room temperature and samples annealed at 1000 °C and 1100 °C) to a solution of Fick's diffusion equation for an initial Gaussian profile by Malherbe et al. [44]. The fitted spectra are shown in Fig. 12 (a), (b), and (c), for the as-implanted, 1000, and 1100 °C annealing profiles, respectively. The diffusion coefficients obtained in this work were governed by equations (9) and (10) given in [44] by incorporating the solution for a perfect heat sink at the surface because the Se signals at the surface for these profiles (as-implanted and sample annealed at 1000 °C and 1100 °C) were zero. We obtained 5.9×10^{-20} m^2s^{-1} and 4.79×10^{-20} m^2s^{-1} as the diffusion coefficients for Se diffusion in defective glassy carbon after annealing at 1000 °C and 1100 °C, respectively (see Table 1). Although Fig. 9 shows that there was still some broadening of the profile at 1200 °C, this was within the statistical error of our RBS measurements. Consequently, no reliable diffusion coefficient could be extracted.

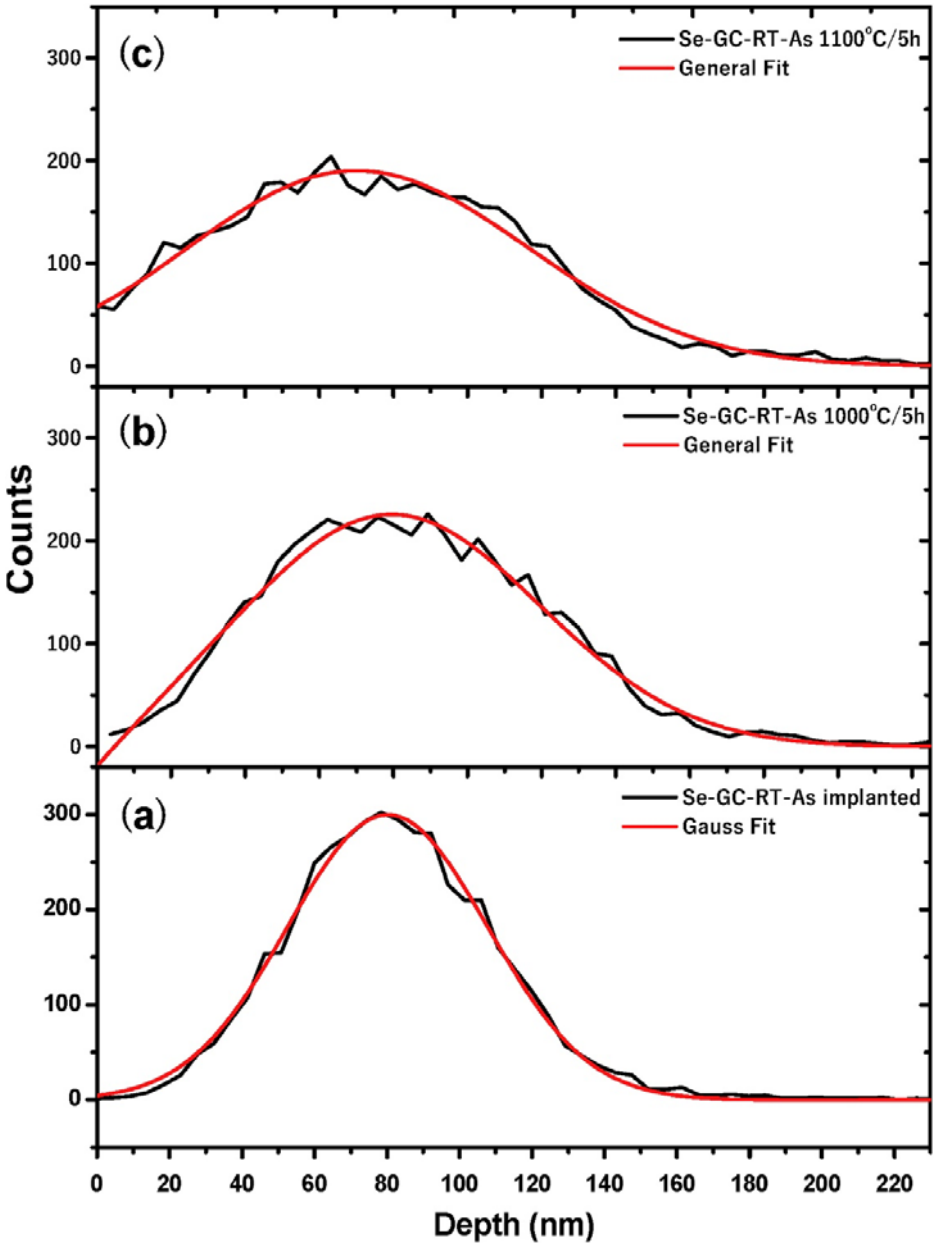

Fig. 12. Examples of fitting of the diffusion equation solution to the depth profiles of the sample (a) as-implanted (b) annealed at 1000 °C for 5 h and (c) annealed at 1100 °C for 5 h.

Table 1. Diffusion coefficients of different ions implanted in glassy carbon.

Implanted ion	Diffusion coefficient (D) (m^2s^{-1})	Annealing temperature (°C)	Annealing duration (hour)	References
Be	3.00×10^{-17}	1285	½	[14]
Be	2.50×10^{-17}	1340	¾	[14]
In	2.15×10^{-17}	300	1	[18]
Cd	7.82×10^{-19}	350	1	[19]
Ag	7.70×10^{-20}	500	1	[21]
Ag	3.70×10^{-20}	550	1	[21]
Ag	5.30×10^{-20}	575	1	[21]
Sr	1.60×10^{-19}	300	1	[21]
Sr	3.70×10^{-19}	400	1	[21]
Se	5.90×10^{-20}	1000	5	this study
Se	4.79×10^{-20}	1100	5	this study

Table 1 compares the diffusion coefficients of Se (this study) and different ions implanted in glassy carbon from previous studies. The diffusion coefficient of Se decreases with increasing annealing temperature, contrary to expectation. The continuous annealing of defects during heat treatment of the sample could be responsible for this. Since the sample was subjected to sequential annealing, one would expect that previous heat treatments will affect the microstructure of the sample and consequently the diffusion coefficients. A similar decrease in diffusion coefficients with annealing temperature has been reported for the diffusion of Ag in glassy carbon [21]. The decreasing trend in the diffusion coefficients of Be [14] could be due to the different annealing times and annealing temperatures.

The bombardment of different energetic ions can induce radiation damage in the solid material (glassy carbon in this case). While the implanted ions can be trapped by defects at a particular temperature, it is also possible for diffusion to occur above the defects temperature via different diffusion mechanisms [44]. The activation energy (E_a) would be a useful parameter in characterizing the diffusion mechanism. But until now, none has been reported for the diffusion of Se in defective glassy carbon. We have grouped the diffusion of different atomic species in defective glassy carbon with respects to their diffusion coefficients as follows: order of 10^{-17} m^2s^{-1} (Be and In) can be said to exhibit fast diffusion, 10^{-19} m^2s^{-1} (Cd and Sr) intermediate diffusion, and 10^{-20} m^2s^{-1} (Ag and Se) slow diffusion (see Table 1).

4. Conclusions

Raman spectroscopy and Rutherford backscattering spectrometry have been applied to investigate the structural changes and the migration behaviour of Se ion-implanted in glassy carbon after sequential isochronal annealing. Implantation of Se amorphized glassy carbon resulting in an increase in density (from 1.42 to 2.1 gcm^{-3}). No notable diffusion occurred for the sample annealed at the low-temperature regime (300–700 °C). Raman spectroscopy showed limited recrystallization after annealing at the low-temperature regime but recovery of some of the implant damage coupled with out-diffusion was observed after annealing at 1000–1200 °C. The original structure of glassy carbon was not achieved at 1200 °C which shows that some radiation damage was retained within it, giving rise to a different structure other than the pristine glassy carbon. Diffusion coefficients of 5.9×10^{-20} m^2s^{-1} and 4.79×10^{-20} m^2s^{-1} were obtained for Se in defective glassy carbon at 1000 and 1100 °C,

respectively. More diffusion studies will be required to obtain more values of diffusion coefficients. Such studies should be done in the limited temperature range (1000–1100 °C) where diffusion coefficients were earlier obtained. By doing so, adequate points (i.e. the diffusion coefficient values) would be available to obtain activation energy needed to adequately characterize the diffusion of the Se in defective glassy carbon.

Declaration of competing interest

The authors declare that they have no known competing financial interests or personal relationships that could have appeared to influence the work reported in this paper.

Acknowledgment

The authors appreciate Prof. Jackie Nel at the University of Pretoria, South Africa, Prof. Elke Wendler, and the technical staff at the Institut für Festkörperphysik, Friedrich-Schiller-Universität Jena, Germany, for their assistance during part of the experiment.

References

[1] J.B. Malherbe, O.S. Odutemowo, E.G. Njoroge, D.F. Langa, T.T. Hlatshwayo, C. C. Theron, Ion bombardment of glassy carbon, Vacuum 149 (2018) 19–22, https://doi.org/10.1016/j.vacuum.2017.11.006.
[2] P.J.F. Harris, Fullerene-related structure of commercial glassy carbons, Philos. Mag. 84 (2004) 3159–3167, https://doi.org/10.1080/14786430410001720363.
[3] O.S. Odutemowo, J.B. Malherbe, L.C. Prinsloo, E.G. Njoroge, R. Erasmus, E. Wendler, A. Undisz, M. Rettenmayr, Structural and surface changes in glassy carbon due to strontium implantation and heat treatment, J. Nucl. Mater. 498 (2018) 103–116, https://doi.org/10.1016/j.jnucmat.2017.10.018.
[4] C.E. Plock, J. Vasquez, Use of glassy carbon as a working electrode in controlled potential coulometry, Talanta 16 (1969) 1490–1492, https://doi.org/10.1016/0039-9140(69)80204-3.
[5] N.L. Pocard, D.C. Alsmeyer, R.L. McCreery, T.X. Neenan, M.R. Callstrom, Doped glassy carbon: a new material for electrocatalysis, J. Mater. Chem. 2 (1992) 771–784.
[6] S. Sharma, Glassy Carbon: a promising material for micro and nanomanufacturing, Materials (Basel) 11 (2018) 1–21, https://doi.org/10.3390/ma11101857.
[7] M.A. Angle, G.E. Blair, C.C. Maier, Method of moulding glass lenses, United States Patent (19) (1974) 1–10, 3833347, https://patents.google.com/patent/US3833347. (Accessed 22 December 2020).
[8] E.E. Hucke, R.A. Fuys, R.G. Craig, Glassy carbon: a potential dental implant Material, J. Biomed. Mater. Res. Symposium. 274 (1973) 263–274, https://doi.org/10.1002/jbm.820070318.
[9] N. Tokiti, I. Michio, Y. Shigehiko, A comment on glassy carbon, Bull. Chem. Soc. (1968) 3023–3024, https://doi.org/10.1246/BCSJ.41.3023.
[10] S. Yamada, A review of glasslike carbons, DCIC Report 68–2 (1968) 1–39. https://apps.dtic.mil/dtic/tr/fulltext/u2/668465.pdf. (Accessed 20 January 2020).
[11] Hochtemperatur-werkstoffe GmbH, Germany, properties of glassy carbon. http://www.htw-germany.com/technology.php5?lang=en&nav0=2. (Accessed 19 February 2020).
[12] P.J.F. Harris, S.C. Tsang, High-resolution electron microscopy studies of non-raphitizing

carbons, Philos. Mag. A Phys. Condens. Matter, Struct. Defects Mech. Prop. 76 (1997) 667–677, https://doi.org/10.1080/01418619708214028.
[13] S.S. Bukalov, L.A. Leites, A.I. Sorokin, A.S. Kotosonov, Structural changes in industrial glassy carbon as a function of heat treatment temperature according to Raman spectroscopy and X-ray diffraction data, Nano: Phys., Chem., Math. 5 (2014) 186–191.
[14] O. Koskelo, U. K¨oster, I. Riihim¨aki, J. R¨ais¨anen, Migration kinetics of ion-implanted beryllium in glassy carbon, Diam. Relat. Mater. 17 (2008) 1991–1993, https://doi.org/10.1016/j.diamond.2008.06.002.
[15] D.F. Langa, N.G. Van Der Berg, E. Friedland, J.B. Malherbe, A.J. Botha, P. Chakraborty, E. Wendler, W. Wesch, Heat treatment of glassy carbon implanted with cesium at room and high temperatures, Nucl. Instrum. Methods Phys. Res. Sect. B Beam Interact. Mater. Atoms 273 (2012) 68–71, https://doi.org/10.1016/j.nimb.2011.07.041.
[16] O.S. Odutemowo, J.B. Malherbe, C.C. Theron, E.G. Njoroge, E. Wendler, In-situ RBS studies of strontium implanted glassy carbon, Vacuum 126 (2016) 101–105, https://doi.org/10.1016/j.vacuum.2016.01.024.
[17] O.S. Odutemowo, J.B. Malherbe, L. Prinsloo, D.F. Langa, E. Wendler, High temperature annealing studies of strontium ion implanted glassy carbon, Nucl. Instrum. Methods Phys. Res. Sect. B Beam Interact. Mater. Atoms 371 (2016) 332–335, https://doi.org/10.1016/j.nimb.2015.10.054.
[18] E.G. Njoroge, L.D. Sebitla, C.C. Theron, M. Mlambo, T.T. Hlatshwayo, O. S. Odutemowo, V.A. Skuratov, E. Wendler, J.B. Malherbe, Structural modification of indium implanted glassy carbon by thermal annealing and SHI irradiation, Vacuum 144 (2017) 63–71, https://doi.org/10.1016/j.vacuum.2017.07.020.
[19] T.T. Hlatshwayo, L.D. Sebitla, E.G. Njoroge, M. Mlambo, J.B. Malherbe, Annealing effects on the migration of ion-implanted cadmium in glassy carbon, Nucl. Instrum. Methods Phys. Res. Sect. B Beam Interact. Mater. Atoms 395 (2017) 34–38, https://doi.org/10.1016/j.nimb.2017.01.086.
[20] M.Y.A. Ismail, J.B. Malherbe, O.S. Odutemowo, E.G. Njoroge, T.T. Hlatshwayo, M. Mlambo, E. Wendler, Investigating the effect of heat treatment on the diffusion behaviour of xenon implanted in glassy carbon, Vacuum 149 (2018) 74–78, https://doi.org/10.1016/j.vacuum.2017.12.021.
[21] O.S. Odutemowo, M.S. Dhlamini, E. Wendler, D.F. Langa, M.Y.A. Ismail, J. B. Malherbe, Effect of heat treatment on the migration behaviour of Sr and Ag CO-implanted in glassy carbon, Vacuum 171 (2020) 109027, https://doi.org/10.1016/j.vacuum.2019.109027.
[22] A.J. Innocent, T.T. Hlatshwayo, E.G. Njoroge, J.B. Malherbe, Interface interaction of tungsten film deposited on glassy carbon under vacuum annealing, Vacuum 148 (2018) 113–116, https://doi.org/10.1016/j.vacuum.2017.11.020.
[23] A.J. Innocent, T.T. Hlatshwayo, E.G. Njoroge, T.P. Ntsoane, M. Madhuku, E. O. Ejeh, M. Mlambo, M.Y.A. Ismail, C.C. Theron, J.B. Malherbe, Evaluation of diffusion parameters and phase formation between tungsten films and glassy carbon, Vacuum 175 (2020) 109245, https://doi.org/10.1016/j.vacuum.2020.109245.
[24] A.L. Nichols, D.L. Aldama, M. Valleti, Handbook of Nuclear Data for Safeguards, IAEA Nuclear Data Section, INDC (NDS)-0502, Vienna, Austria, 2007, pp. 1–94.
[25] G. Shaw, D. Ashworth, Selenium: radionuclides, Encycl. Inorg. Chem. (2010), https://doi.org/10.1002/0470862106.ia718.
[26] International Commission on Radiological Protection, Nuclear decay data for dosimetric calculations, ICRP Publication 107, Ann. ICRP 38 (2008).
[27] J. Gerhard, S. Hollas, N. Kivel, K. Kossert, S. Van Winckel, C. Lierse, Preparation of radiochemically pure 79Se and highly precise determination of its half-life, J. Appl. Rad. Isot. 68 (2010) 2339–2351, https://doi.org/10.1016/j.apradiso.2010.05.006.

[28] F. Fordyce, Selenium geochemistry and health, Ambio 36 (2007) 94–97, https://doi.org/10.2307/4315793.
[29] L.W. Jacobs, Selenium in agriculture and the environment, in: Am. Soc. Agron. Soil Sci. Soc. Am., 1989, pp. 37–65, https://doi.org/10.1016/0167-8809(84)90047-1.
[30] J. Peterson, M. MacDonell, L. Haroun, F. Monette, R.D. Hildebrand, A. Taboas, Radiological and Chemical Fact Sheets to Support Health Risk Analyses for Contaminated Areas, Argonne National Lab, EVS, 2005, pp. 1–133. http://www.nuceng.ca/refer/radiation/anl-factsheets.pdf%5Cnpapers2://publication/uuid/4ABDB82D-0580-4E66-A891-DFBF74A7FA94.
[31] T. Hlatshwayo, Diffusion of Silver in 6H-SiC, University of Pretoria, Pretoria, South Africa, 2010. http://upetd.up.ac.za/thesis/available/etd-06182011-165556/.
[32] J.F. Ziegler, M.D. Ziegler, J.P. Biersack, SRIM - the stopping and range of ions in matter (2010), Nucl. Instrum. Methods Phys. Res. Sect. B Beam Interact. Mater. Atoms 268 (2010) 1818–1823, https://doi.org/10.1016/j.nimb.2010.02.091.
[33] M. Iwaki, Estimation of the atomic density of amorphous carbon using ion implantation, SIMS and RBS, Surf. Coating. Technol. 158–159 (2002) 377–381, https://doi.org/10.1016/S0257-8972(02)00247-5.
[34] A.J. McKenna, T. Trevethan, C.D. Latham, P.J. Young, M.I. Heggie, Threshold displacement energy and damage function in graphite from molecular dynamics, Carbon N. Y. 99 (2016) 71–78, https://doi.org/10.1016/j.carbon.2015.11.040.
[35] S. Prawer, F. Ninio, I. Blanchonette, Raman spectroscopic investigation of ion-beam-irradiated glassy carbon, J. Appl. Phys. 68 (1990) 2361–2366, https://doi.org/10.1063/1.346547.
[36] A.C. Ferrari, J. Robertson, Interpretation of Raman spectra of disordered and amorphous carbon, Phys. Rev. B 61 (2000) 14095–14107, https://doi.org/10.1136/ip.2010.029215.730.
[37] K. Jurkiewicz, M. Pawlyta, D. Zygadło, D. Chrobak, S. Duber, R. Wrzalik, A. Ratuszna, A. Burian, Evolution of glassy carbon under heat treatment: correlation structure–mechanical properties, J. Mater. Sci. 53 (2018) 3509–3523, https://doi.org/10.1007/s10853-017-1753-7.
[38] M.A. Pimenta, G. Dresselhaus, M.S. Dresselhaus, L.G. Cançado, A. Jorio, R. Saito, Studying disorder in graphite-based systems by Raman spectroscopy, Phys. Chem. Chem. Phys. 9 (2007) 1276–1291, https://doi.org/10.1039/b613962k.
[39] A.C. Ferrari, Raman spectroscopy of graphene and graphite: disorder, electron-phonon coupling, doping and nonadiabatic effects, Solid State Commun. 143 (2007) 47–57, https://doi.org/10.1016/j.ssc.2007.03.052.
[40] F. Tuinstra, J.L. Koenig, Raman spectrum of graphite, J. Chem. Phys. 53 (1970) 1126–1130, https://doi.org/10.1063/1.1674108.
[41] V. Lavrentiev, J. Vacik, H. Naramoto, Structural phenomena in glassy carbon induced by cobalt ion implantation, Appl. Phys. Mater. Sci. Process 92 (2008) 673–680, https://doi.org/10.1007/s00339-008-4615-y.
[42] W.K. Burton, N. Cabrera, F.C. Frank, The growth of crystals and the equilibrium structure of their surfaces, Philos. Trans. R. Soc. A. 243 (1951) 299–358, https://doi.org/10.1098/rsta.1951.0006.
[43] D.G. McCulloch, S. Prawer, The effect of annealing and implantation temperature on the structure of C ion - beam - irradiated glassy carbon, J. Appl. Phys. 78 (1995) 3040–3047, https://doi.org/10.1063/1.360054.
[44] J.B. Malherbe, P.A. Selyshchev, O.S. Odutemowo, C.C. Theron, E.G. Njoroge, D. F. Langa, T.T. Hlatshwayo, Diffusion of a mono-energetic implanted species with a Gaussian profile, Nucl. Instrum. Methods Phys. Res. Sect. B Beam Interact. Mater. Atoms 406 (2017) 708–713, https://doi.org/10.1016/j.nimb.2017.04.067.